Int J Legal Med
DOI 10.1007/s00414-016-1454-9

ORIGINAL ARTICLE

Post-mortem CT: Hounsfield unit profiles obtained in the lungs with respect to the cause of death assessment

Daniel Schober[1] · **Nicole Schwendener**[1] · **Wolf-Dieter Zech**[1] · **Christian Jackowski**[1]

Received: 4 April 2016 / Accepted: 15 September 2016

Abstract Segmentation of the lungs using post-mortem computed tomography (PMCT) data was so far not feasible due to post-mortem changes such as internal livores. Recently, an Osirix plug-in has been developed allowing automatically segmenting lungs also in PMCT data. The aim of this study was to investigate if the Hounsfield unit (HU) profiles obtained in PMCT data of the segmented lung tissue present with specific behaviour in relation to the cause of death. In 105 PMCT data sets of forensic cases, the entire lung volumes were segmented using the Mia Lite plug-in on Osirix. HU profiles of the lungs were generated and correlated to cause of death groups as assessed after forensic autopsy (cardiac death, fatal haemorrhage, craniocerebral injury, intoxication, drowning, hypothermia, hanging and suffocation). Especially cardiac death cases, intoxication cases, fatal haemorrhage cases and hypothermia cases showed very specific HU profiles. In drowning, the profiles showed two different behaviours representing wet and dry drowning. HU profiles rather varied in craniocerebral injury cases, hanging cases as well as in suffocation cases. HU profiles of the lungs segmented from PMCT data may support the cause of death diagnosis as they represent specific morphological changes in the lungs such as oedema, congestion or blood loss. Especially in cardiac death, intoxication, fatal haemorrhage, hypothermia and drowning cases, HU profiles may be very supportive for the forensic pathologist.

Keywords Postmortem CT · Lungs · Automatic segmentation · Cause of death · HU profile

Introduction

Post-mortem computed tomography (PMCT) imaging has experienced an increasing distribution into forensic post-mortem investigations. Being a non-invasive investigation tool, it has proven useful as an additional instrument in the investigation of forensic cases mostly in combination with legal autopsy [1–7]. Several studies have shown that PMCT can provide additional information especially in the detection of skeletal fractures [4, 8], gas accumulation in organs [9] or decay [10]. Furthermore, it has already been supportive in identifying corpses [11, 12]. PMCT has the major advantage that the data can be easily stored, transmitted and findings, if necessary, retrospectively reconstructed. PMCT can also support the autopsy by providing information on the expected findings in advance, so that the autopsy techniques may be adapted to better document the findings or even not to miss the findings at all [2].

As the clinical autopsy rates have declined worldwide in the last decades [13], post-mortem imaging may also has the potential to act as an alternative post-mortem examination technique in clinical pathology [14, 15]. There is also a growing demand for minimal invasive procedures in the society, among others notably for religious reasons [16].

Until recently, semi-automatic segmentation of the lungs in PMCT was nearly impossible. Due to a regular post-mortem phenomenon namely the sedimentation of blood components, the so-called internal livores, simply Hounsfield unit (HU)-based segmentation tools did not perform well under post-mortem conditions because segmentation was based on a specific radiopacity range given in HU, which did not work

✉ Christian Jackowski
christian.jackowski@irm.unibe.ch

1 Institute of Forensic Medicine, University of Bern, Bühlstr. 20, CH-3012 Bern, Switzerland

Published online: 20 October 2016

in depending lung areas. With the newly developed freeware "Mia Lite", available as Osirix plug-in, a semi-automatic segmentation of organs including the lungs can be realized within a few minutes. The segmented lung volume can then be used for further examinations, such as the investigation of HU values within the segmented volume.

We hypothesized that the mean distribution of HU values within the segmented lung volume may be depending on the individual cause of death and investigated whether there are differences in the HU values given as a HU profile between different causes of death groups.

Materials and methods

Study population

One hundred forty-seven PMCT data sets of forensic cases were prospectively enrolled and scanned successively. All cases were forensic corpses who underwent a PMCT prior to the autopsy ordered by the local authorities. A number of 42 (28.57 %) cases were excluded after the PMCT scan due to the following exclusion criteria: metallic artefacts within the region of interest ($n = 14$), advanced putrefaction of the lung ($n = 14$), open chest trauma ($n = 6$) and haematothorax ($n = 8$). The first would have affected the HU measurements and the others would have disturbed semi-automatic segmentation. One hundred five cases finally were evaluated with respect to the study question.

The age at death of the analysed 105 cases ranged from 1 month to 89 years (mean 52.3 years, standard deviation ±19.75 years; 68 males, 37 females). The post-mortem interval, which was defined as the time period between estimated time of death and PMCT data acquisition, ranged between 1–2 h and several days (see Table 1).

PMCT

All PMCT scans were performed with the bodies in supine position wrapped either in body bags or in sheets of linen. The examinations were performed on a six-detector row system (Somatom Emotion 6, Siemens Medical, Erlangen, Germany) with the following raw data acquisition parameters: 130 kV, 90 mAS and 1 mm collimation and the following image reconstruction parameters: thickness 1.25 mm, increment 0.6 mm, FoV 500 mm and reconstruction kernel B70s.

Image analysis

All PMCT data sets were transferred to a personal computer running MacPro with Osirix [17]. Using semi-automatic plotting with Mia Lite [18], which is used as a plug-in in Osirix, a 3D image of the lung was created and the lung volume was segmented using an integrated standard volume rendering procedure. The voxel volume was 1.2 mm^3 (field of view 500 × 500 mm, slice thickness 1.25 mm, image matrix of 512 × 512 pixels). The main bronchial cavity and the mediastinum were blocked manually to prevent that these areas would have been integrated into the segmented lung volumes. Mia Lite also worked with HU thresholds to be set individually (Fig. 1). In Mia Lite, these thresholds work not as fixed limits for the segmentation, but rather as a clue for the program to exclude irrelevant areas as for example pleural fluids. HU values above or beneath these thresholds are still included in the segmented volume when the voxels were within the aimed anatomic region. For the lung segmentation in PMCT data, thresholds were chosen between an upper value of 20 HU and a lower one of −1112 HU in order to include a maximum of lung volume. The ideal limits were chosen for each dataset individually based on empirical experience and adapted based on the case individual performance. After segmentation with Mia Lite in Osirix, the segmentation was manually checked for accuracy. The total of the segmented voxels was then transferred to a personal computer (Windows 8) equipped with Matlab, where a 2D graph showing the radiopacity distribution within the lung, the so-called HU profile, was created. Subsequently, the coordinates of the graphs were transferred to Excel, where all curves were compared and classified according to the cause of death. Based on this data, a mean distribution curve for the individual cause of death groups was created. The mean distribution was calculated using the X- and Y-values from the graphs corresponding to the individual cases generated in Matlab, which were exported to Microsoft Excel. Subsequently, the mean of all Y-values (amount of voxel) corresponding to a specific X-value (HU from −1500HU to +1000HU) was calculated and mapped in a mean distribution. This was done for every cause of death individually.

Results

The following cause of death groups were composed based on the autopsy assessment: cardiac death ($n = 34$), fatal haemorrhage ($n = 21$), craniocerebral injury with central regulatory failure ($n = 23$), intoxication ($n = 8$), drowning ($n = 7$), hypothermia ($n = 4$), hanging ($n = 4$) and suffocation ($n = 4$).

Cardiac death

The cardiac death cases ($n = 34$) presented with a broad distribution of the HU values covering the entire spectrum from −1000 HU up to 50 HU (Fig. 2a). Some of the individual profiles were characterized by a double peak appearance with a peak at lower values (−880 HU and −630 HU) and a second peak at higher values (−400 HU and −10 HU). A convergence of the individual profiles could be seen between −800 HU and −400 HU.

The mean cardiac death case profile presented a broad bell-shaped curve covering almost all negative HU value ranges

Table 1 Synopsis of all cases. Visualizing CT-Nr., upper HU limit, lower HU limit, sex, age, weight in kilogram, height in centimetres, BMI in kilogram per metre squared, the lung weight in gram and cause of death for each case

CT-Nr.	Upper limit	Lower limit	Sex	Age	Weight (kg)	Height (cm)	BMI	Lung weight (g)	Post-mortem interval (h)	Cause of death
1	−50	−1112	Male	39	70	173	23.4	1680	48 to 72	Cardiac death (acute cardiac failure due to cardiac infarction)
2	−120	−1112	Female	43	58	150	25.8	1060	48 to 72	Intoxication (street heroin and dormicum)
3	−105	−1112	Male	35	55	174	18.2	1420	3 to 6	Craniocerebral injury with central regulatory failure (brain haemorrhage due to head contusion)
4	−91	−1112	Female	74	86	163	32.4	1540	48 to 72	Craniocerebral injury with central regulatory failure (collision as a pedestrian with a car, followed by CPR)
5	−120	−1112	Male	21	81	183	24.2	940	3 to 6	Suffocation (combination with heat exposure due to fire)
6	18	−1112	Female	17	73	170	25.3	1200	13 to 24	Cardiac death (acute cardiac failure due to multiple lung embolism, followed by CPR)
7	−90	−1112	Male	34	103	192	27.9	1625	7 to 12	Intoxication (hydromorphon, amitriptylin and duloxetin)
8	−15	−1112	Male	55	128	178	40.4	1870	3 to 6	Cardiac death (cardiac failure due to precursory infarction and coronary sclerosis, followed by CPR)
9	−120	−1112	Female	56	70	171	23.9	770	3 to 6	Craniocerebral injury with central regulatory failure (collision as a pedestrian with a car)
10	−120	−1112	Female	52	78	170	27.0	1610	48 to 72	Intoxication (with alcohol (3.8 per mill)
11	0	−1112	Male	89	80	170	27.7	1520	48 to 72	Cardiac death (collision as pedestrian with a car, acute cardiac failure due to fat embolism in the lung)
12	−10	−1112	Female	54	78	156	32.1	800	1 to 2	Cardiac death (collision as pedestrian with a car, cardiac failure due to precursory damage, followed by CPR)
13	−20	−1112	Female	30	100	174	33.0	1030	1 to 2	Cardiac death (acute cardiac failure caused by pericardial tamponade)
14	−30	−1112	Male	84	74	172	25.0	900	3 to 6	Cardiac death (acute cardiac failure due to cardiac infarction and coronary sclerosys)
15	−120	−1112	Female	84	47	154	19.8	870	3 to 6	Cardiac death (cardiac failure due to cardiac infarction and coronary sclerosys)
16	20	−1112	Male	23	66	185	19.3	1900	3 to 6	Cardiac death (cardiac failure due to precursory cardiac damage)
17	−60	−1112	Male	44	80	180	24.7	1210	48 to 72	Cardiac death (acute cardiac failure due to pericardial tamponade, caused by aortic dissection)
18	−50	−1112	Female	79	88	162	33.5	1400	3 to 6	Cardiac death (acute cardiac failure due to cardiac infarction)
19	−80	−1112	Female	51	70	165	25.7	620	1 to 2	Craniocerebral injury with central regulatory failure (spine near skull fracture after jump from a bridge)
20	−50	−1112	Female	48	74	173	24.7	1130	3 to 6	Cardiac death (position-depending cardiovascular failure after fall)
21	−20	−1112	Male	23	62	177	19.8	1594	24 to 48	Craniocerebral injury with central regulatory failure (respiratory paralysis after traumatic head injury)
22	−80	−1112	Male	33	90	178	28.4	1670	13 to 24	Intoxication (central respiratory paralysis due to mixed intoxication with amphetamine, heroin, ecstasy and cocaine)
23	−90	−1112	Male	62	81	182	24.5	1420	3 to 6	Cardiac death (acute cardiac failure due to fresh septum infarction and precursory cardiac damage, followed by CPR)
24	−140	−1112	Female	62	45	170	15.6	750	48 to 72	Fatal haemorrhage (cut trough A. brachialis and V. brachialis in suicidal intention)
25	−90	−1112	Male	57	70	177	22.3	1000	1 to 2	Drowning (dry drowning)
26	−120	−1112	Male	56	88	176	28.4	1550	3 to 6	Cardiac death (acute cardiac failure due to air embolism caused by an accident with a truck)
27	−120	−1112	Female	76	78	164	29.0	1023	3 to 6	Craniocerebral injury with central respiratory failure (intracranial bleeding due to fall)
28	−100	−1112	Female	44	54	154	22.8	1200	13 to 24	Intoxication (mixed intoxication with methadone heroin and cocaine followed by respiratory paralysis)

Table 1 (continued)

CT-Nr.	Upper limit	Lower limit	Sex	Age	Weight (kg)	Height (cm)	BMI	Lung weight (g)	Post-mortem interval (h)	Cause of death
29	−100	−1112	Male	52	70	177	22.3	1070	13 to 24	Hypothermia (followed by CPR)
30	−120	−1112	Male	79	81	174	26.8	1160	48 to 72	Hypothermia
31	−130	−1112	Male	77	89	179	27.8	1045	3 to 6	Craniocerebral injury with central regulatory failure (due to a shot to the head)
32	−80	−1112	Male	42	88	178	27.8	1470	48 to 72	Hanging
33	−100	−1112	Male	69	90	171	30.8	1831	>72	Drowning (wet drowning, followed by CPR)
34	−120	−1112	Male	62	50	171	17.1	850	24 to 48	Fatal haemorrhage (after shot to the head)
35	−120	−1112	Female	49	71	170	24.6	900	3 to 6	Cardiac death (acute cardiac failure after traffic accident due to cardiac infarction and loss of blood, followed by CPR)
36	−120	−1112	Male	65	80	173	26.7	900	24 to 48	Craniocerebral injury with central regulatory failure (due to ski accident, followed by CPR)
37	−90	−1112	Female	48	64	168	22.7	995	48 to 72	Craniocerebral injury with central regulatory failure (due to brain oedema and subdural bleeding after fall)
38	−120	−1112	Male	63	90	170	31.1	990	48 to 72	Cardiac death (acute cardiac failure due to cardiac infarction)
39	−100	−1112	Female	64	60	163	22.6	1240	3 to 6	Craniocerebral injury with central regulatory failure (brain haemorrhage due to head contusion)
40	−120	−1112	Female	61	52	174	17.2	1180	>72	Suffocation (caused by a acute asthma attack)
41	−120	−1112	Male	58	70	173	23.4	1080	7 to 12	Fatal haemorrhage (after fall and multiple cuts among others A. facialis)
42	−120	−1112	Male	74	90	176	29.1	1400	3 to 6	Craniocerebral injury with central regulatory failure (due to gunshot to the heat)
43	−120	−1112	Female	87	62	168	22.0	1390	1 to 2	Cardiac death (acute cardiac failure due to cardiac infarction)
44	−50	−1112	Male	44	93	186	26.9	1380	26 to 28	Cardiac death (acute cardiac failure, after re-infarction during stenting, followed by CPR)
45	−60	−1112	Male	78	70	174	23.1	2584	3 to 6	Cardiac death (acute cardiac failure due to cardiac infarction)
46	−110	−1112	Female	87	79	165	29.0	630	13 to 24	Fatal haemorrhage (due to internal bleeding after collision as pedestrian with a car)
47	−120	−1112	Male	30	78	191	21.4	1340	24 to 48	Fatal haemorrhage (due to traumatic aorta rupture)
48	−120	−1112	Female	73	65	166	23.6	790	3 to 6	Suffocation (due to CO poisoning)
49	−120	−1112	Male	48	104	175	34.0	910	13 to 24	Craniocerebral injury with central regulatory failure (traumatic spine injury)
50	−120	−1112	Female	53	44	165	16.2	770	7 to 12	Intoxication (central regulatory failure due to alcohol intoxication)
51	−120	−1112	Male	46	65	170	22.5	770	13 to 24	Cardiac death (cardiac failure due to precursory cardiac damage)
52	−120	−1112	Male	16	77	176	24.9	1140	>72	Cardiac death (acute cardiac failure due to cardiac arrythmia caused by high voltage current)
53	−120	−1112	Female	38	66	164	24.5	1120	7 to 12	Hanging (followed by CPR)
54	−80	−1112	Male	48	115	193	30.9	2000	3 to 6	Craniocerebral injury with central regulatory failure (fall from 5 m height)
55	−80	−1112	Female	65	50	162	19.1	800	>72	Fatal haemorrhage (after gunshot to the head)
56	−120	−1112	Male	18	67	173	22.4	640	24 to 48	Fatal haemorrhage (after collision as a pedestrian with a car)
57	−90	−1112	Male	48	80	170	27.7	1288	7 to 12	Cardiac death (acute cardiac failure due to cardiac infarction, followed by CPR)
58	−50	−1112	Male	14	45	160	17.6	655	3 to 6	Fatal haemorrhage (due to craniocerebral injury)
59	−120	−1112	Male	53	98	184	28.9	1910	24 to 48	Cardiac death (cardiac failure due to precursory cardiac damage)
60	−120	−1112	Male	43	78	177	24.9	1111	3 to 6	Drowning (dry drowning)
61	−120	−1112	Male	50	108	178	34.1	710	48 to 72	Fatal haemorrhage (after thorax trauma)
62	−150	−1112	Male	51	60	173	20.0	908	13 to 24	Fatal haemorrhage (after gunshot to the head)

Table 1 (continued)

CT-Nr.	Upper limit	Lower limit	Sex	Age	Weight (kg)	Height (cm)	BMI	Lung weight (g)	Post-mortem interval (h)	Cause of death
63	−120	−1112	Female	40	75	168	26.6	630	24 to 48	Fatal haemorrhage (after two gunshots to the thorax)
64	−120	−1112	Male	74	85	172	28.7	1267	48 to 72	Hanging
65	−90	−1112	Female	27	120	168	42.5	1000	48 to 72	Cardiac death (acute cardiac failure due to lung embolism, followed by CPR)
66	−120	−1112	Male	62	93	186	26.9	1890	13 to 24	Cardiac death (acute cardiac failure due to precursory cardiac damage, followed by CPR)
67	−110	−1112	Male	77	108	174	35.7	1761	7 to 12	Craniocerebral injury with central regulatory failure (after severe head trauma)
68	−120	−1112	Male	36	85	182	25.7	1089	13 to 14	Fatal haemorrhage (due to traumatic aorta rupture)
69	−100	−1112	Male	81	78	170	27.0	1445	>72	Hypothermia
70	−90	−1112	Female	81	70	166	25.4	1549	3 to 6	Cardiac death (acute cardiac failure due to precursory cardiac damage, followed by CPR)
71	−80	−1112	Male	62	83	181	25.3	1355	>72	Hypothermia
72	−30	−1112	Female	77	46	153	19.7	1190	3 to 6	Cardiac death (cardiac failure due to precursory cardiac insufficiency and pancreas carcinoma)
73	−140	−1112	Male	70	89	177	28.4	1930	3 to 6	Craniocerebral injury with central regulatory failure (due to gunshot to the heat)
74	−80	−1112	Male	48	93	175	30.4	730	3 to 6	Cardiac death (acute cardiac failure due to poly trauma and blood loss)
75	−120	−1112	Male	57	100	187	28.6	1017	13 to 24	Fatal haemorrhage (internal bleeding after ski accident, followed by CPR)
76	−120	−1112	Female	30	52	157	21.1	795	>72	Fatal haemorrhage (internal bleeding after fall and chest trauma)
77	−120	−1112	Male	26	120	190	33.2	920	24 to 48	Fatal haemorrhage (after traumatic aorta rupture, followed by CPR)
78	−120	−1112	Female	63	76	159	30.1	450	3 to 6	Craniocerebral injury with central regulatory failure (due to traumatic spine lesion)
79	−120	−1112	Female	69	84	170	29.1	1173	48 to 72	Craniocerebral injury with central regulatory failure (due to brain oedema after head contusion)
80	−60	−1112	Male	25	82	187	23.4	1500	13 to 24	Cardiac death (acute cardiac failure due to cardiac arrythmia)
81	−50	−1112	Male	60	105	173	35.1	1280	48 to 72	Cardiac death (cardiac failure due to precursory cardiac damage, followed by CPR)
82	−120	−1112	Male	45	85	178	26.8	1210	3 to 6	Cardiac death (acute pericard tamponade due to aortic dissection, followed by CPR)
83	−60	−1112	Male	39	69	174	22.8	1720	3 to 6	Cardiac death (acute cardiac failure due to multiple lung embolism, followed by CPR)
84	−120	−1112	Female	89	70	155	29.1	610	13 to 24	Craniocerebral injury with central regulatory failure (due to gunshot to the head)
85	−90	−1112	Male	76	80	168	28.3	1230	>72	Drowning (dry drowning)
86	−120	−1112	Female	61	58	160	22.7	930	3 to 6	Suffocation (in snow due to ski accident)
87	−120	−1112	Male	72	78	172	26.4	1703	13 to 24	Craniocerebral injury with central regulatory failure (after severe head trauma)
88	−120	−1112	Male	69	85	184	25.1	830	3 to 6	Fatal haemorrhage (after gunshot to the head)
89	−120	−1112	Male	59	96	178	30.3	1350	1 to 2	Fatal haemorrhage (post-operative internal bleeding, followed by CPR)
90	−20	−1112	Male	24	71	175	23.2	1300	13 to 24	Craniocerebral injury with central regulatory failure (after poly trauma as cyclist)
91	−120	−1112	Male	63	80	175	26.1	1170	7 to 12	Intoxication (respiratory paralysis due to intoxication with opiate and alcohol)
92	−120	−1112	Female	51	41	165	15.1	1107	13 to 24	Intoxication (respiratory paralysis due to methadone and morphine intoxication)
93	−100	−1112	Male	37	73	179	22.8	2005	13 to 24	Drowning (wet drowning)

Table 1 (continued)

CT-Nr.	Upper limit	Lower limit	Sex	Age	Weight (kg)	Height (cm)	BMI	Lung weight (g)	Post-mortem interval (h)	Cause of death
94	−120	−1112	Female	38	52	172	17.6	880	48 to 72	Fatal haemorrhage (collision as pedestrian with a train)
95	−120	−1112	Male	54	53	159	21.0	1200	13 to 24	Drowning (dry drowning)
96	−120	−1112	Male	63	103	181	31.4	2277	7 to 12	Craniocerebral injury with central regulatory failure (brain oedema and bleeding after fall)
97	−120	−1112	Male	31	70	180	21.6	1411	13 to 24	Hanging
98	−120	−1112	Female	20	70	170	24.2	990	1 to 2	Drowning (wet drowning)
99	−289	−970	Male	53	79	178	24.9	800	1 to 2	Fatal haemorrhage (multiple stabbing wounds)
100	−123	−950	Male	59	90	191	24.7	1850	13 to 24	Cardiac death (acute cardiac failure due to fat embolism)
101	−135	−940	Male	62	81	174	26.8	974	24 to 48	Fatal haemorrhage (poly trauma after fall)
102	−300	−970	Male	38	67	165	24.6	600	24 to 48	Craniocerebral injury with central regulatory failure (polytrauma after collision as pedestrian with a train)
103	−170	−900	Male	22	81	181	24.7	1470	13 to 24	Cardiac death (acute cardiac failure due to trauma and arrhythmia)
104	−300	−915	Male	25	70	173	23.4	630	24 to 48	Craniocerebral injury with central regulatory failure (after polytrauma as motorcyclist)
105	−280	−930	Female	0.1	4	0.6	–	–	3 to 6	Fatal haemorrhage (after trauma)

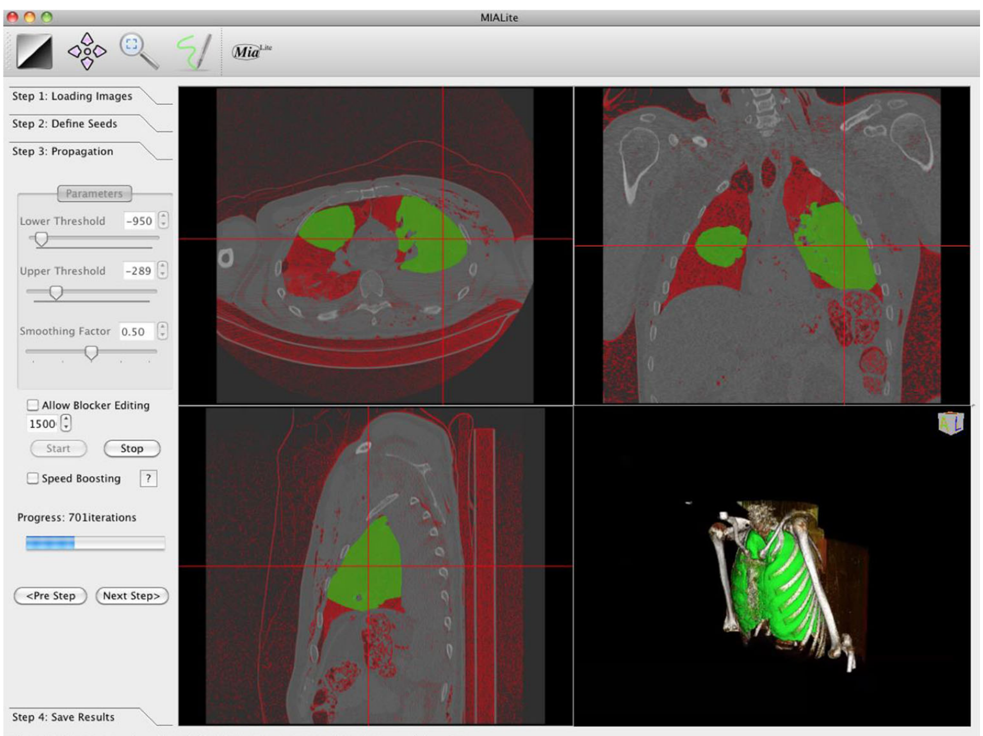

Fig. 1 Screenshot of Mia Lite during segmentation. CT 100, male, age 59 years, weight 90 kg, cardiac death caused by acute cardiac failure due to fat embolism. On the *left*, the HU limits in this case are set to −950 HU as the lower and −289HU as the upper limit. The *red area* corresponds to a region situated between the lower threshold of −950 HU and the upper threshold of −289 HU, which has not been segmented yet. The *green area* represents the area already included by segmentation. The thresholds where defined according to empirical experience and work not as fixed limits for the segmentation, but rather as a clue for the program to exclude irrelevant areas. HU *above* or *beneath* these thresholds are still included in the segmented volume when the voxels were within the aimed anatomic region. *Bottom right* a volume rendering visualization of the segmented lung volume

and showing a plateau between −720 HU and −240 HU (Fig. 3a).

Fatal haemorrhage

The cases of fatal haemorrhage (*n* = 21) presented with a less variable distribution of the HU values (Fig. 2b). The majority of the profiles showed a peak around −900 HU. Even if some of the profiles presented a tiny second elevation at higher values, it was always a dominating peak at very low HU values. There were two exceptions (see Discussion).

The mean distribution (Fig. 3b) showed a sharp concentration of HU values in low radiopacity areas between −1000 HU and −700 HU. After the dominating peak, the curves only decreased slowly between −600 HU till −200 HU, before they reached 0 around 50 HU.

Craniocerebral injury with central regulatory failure

In craniocerebral injury cases (*n* = 23), a wide spectrum of different profiles was observed (Fig. 2c). Most of the curves showed a peak in low radiopacity areas. However, additional peaks at higher HU values (around −200 HU) were also present.

Therefore, the mean distribution curve (Fig. 3c) did show a rather steady decrease between −500 HU and −100 HU after the peak between −1000 and −700.

Intoxication

The intoxication cases (*n* = 8) showed a concentration between −800 HU and −400 HU and therefore demonstrated a shift of the values to higher radiopacity areas (Fig. 2d). There was one exception (CT 92), which will be discussed later on.

The mean curve (Fig. 3d) showed a broad peak at −750 HU and a rather slow decrease.

Drowning

The curves in drowning cases (*n* = 7) showed two different appearances (Fig. 2e). Four of them, representing the cases of dry drowning, presented with a more or less peaky consolidation at lower values whereas three of them, representing the wet drowning cases, rather formed a bell-shaped curve dominating HU areas between −500 and −400. None of the distributions showed two peaks.

Therefore, the mean distribution curve (Fig. 3e) was composed of these two appearances and showed a steep rise of values to a maximum at −850 HU, followed by a gradual decrease of voxels to 0.

Hypothermia

The cases of hypothermia (*n* = 4) showed a rather homogenous distribution (Fig. 2f). The main peak was between −880 HU and −790 HU in all the graphs. CT 69 and CT 71 presented a minor second peak at around −200 HU. CT 29 decreased quickly after the peak, whereas CT 30 gradually decreased afterwards.

The mean distribution of the hypothermia cases (Fig. 3f) showed a pointed peak at −880 HU with a steep rise and fall. Between −550 HU and 100 HU, a plateau was formed at only 20000 voxels.

Hanging

Hanging as cause of death (*n* = 4) showed a very varying appearance (Fig. 2g). For example, CT 97 had a peak at −850 HU, and no second peak or CT 32 had a first peak at −780 HU and a second one at −120 HU. CT 53 showed a bell-shaped distribution around the peak at −500 HU. CT 64 presented with a rise of values to a maximum at −800 HU followed by a plateau with only little decrease till −320 HU.

The mean distribution (Fig. 3g) showed a peak at −820 HU and an accumulation of values at −240 HU.

Fig. 2 HU properties in the lungs of all study cases. In each case, the *x-axis* corresponds to the value of HU; the *y-axis* corresponds to the amount of voxels with a certain HU value. **a** Cardiac death *n* = 34. The *highlighted lines* are CT 35 cardiac failure due to loss of blood, in the context of a traffic accident and CT 44 cardiac failure after re-infarction while stenting. **b** Fatal haemorrhage *n* = 21. Noticeable the amount of voxel with a specific HU is 10 times higher than in the cardiac death cases. The *highlighted lines* are CT 75, a fatal haemorrhage after a skiing accident and CT 77, a fatal haemorrhage after thoracic aortic rupture. No shift of values to a lower density area can be observed, even though a massive internal blood loss could be expected. **c** Craniocerebral injury with central regulatory failure *n* = 23. Very different profiles were present within these 23 cases. In contrast to the fatal haemorrhage cases, several distributions showed two peaks and there was an accumulation of HU values in an area of lower and higher density. **d** Intoxication *n* = 8. The mean distribution showed a shift of HU values to higher radiopacity levels especially when compared to hypothermia or the fatal haemorrhage cases. CT 92 showed an exceptional behaviour with more than 250,000 voxels at around −850 HU, which was more than twice as much compared to a specific HU range of the other profiles, which could be interpreted as lack of pulmonary oedema. **e** Drowning *n* = 7. Noticeably, these cases presented with two case profiles. Four peaks were situated in low-density areas (*thin line*) where as three peaks could be found in high-density areas (*bold line*). The four corresponded to dry drowning cases, as the three were cases of wet drowning. **f** Hypothermia *n* = 4. The mean HU curve was dominated by a distinctive peak around −800 HU comparable to the fatal haemorrhage cases. CT 69 and CT 71 presented a minor second peak at around −200 HU. CT 29 decreased quickly after the peak, whereas CT 30 gradually decreased afterwards. **g** Hanging *n* = 4. These cases showed a very varying appearance with no clear tendency. **h** Suffocation *n* = 4. Again, these cases showed rather varying curves. CT 40 and CT 48 appeared rather similar with a peak at −890 HU and a plateau with little decrease of values between −570 HU and −240 HU. CT 5 and CT 86 had a rather bell-shaped peak at −650 HU and −550 HU, respectively ▶

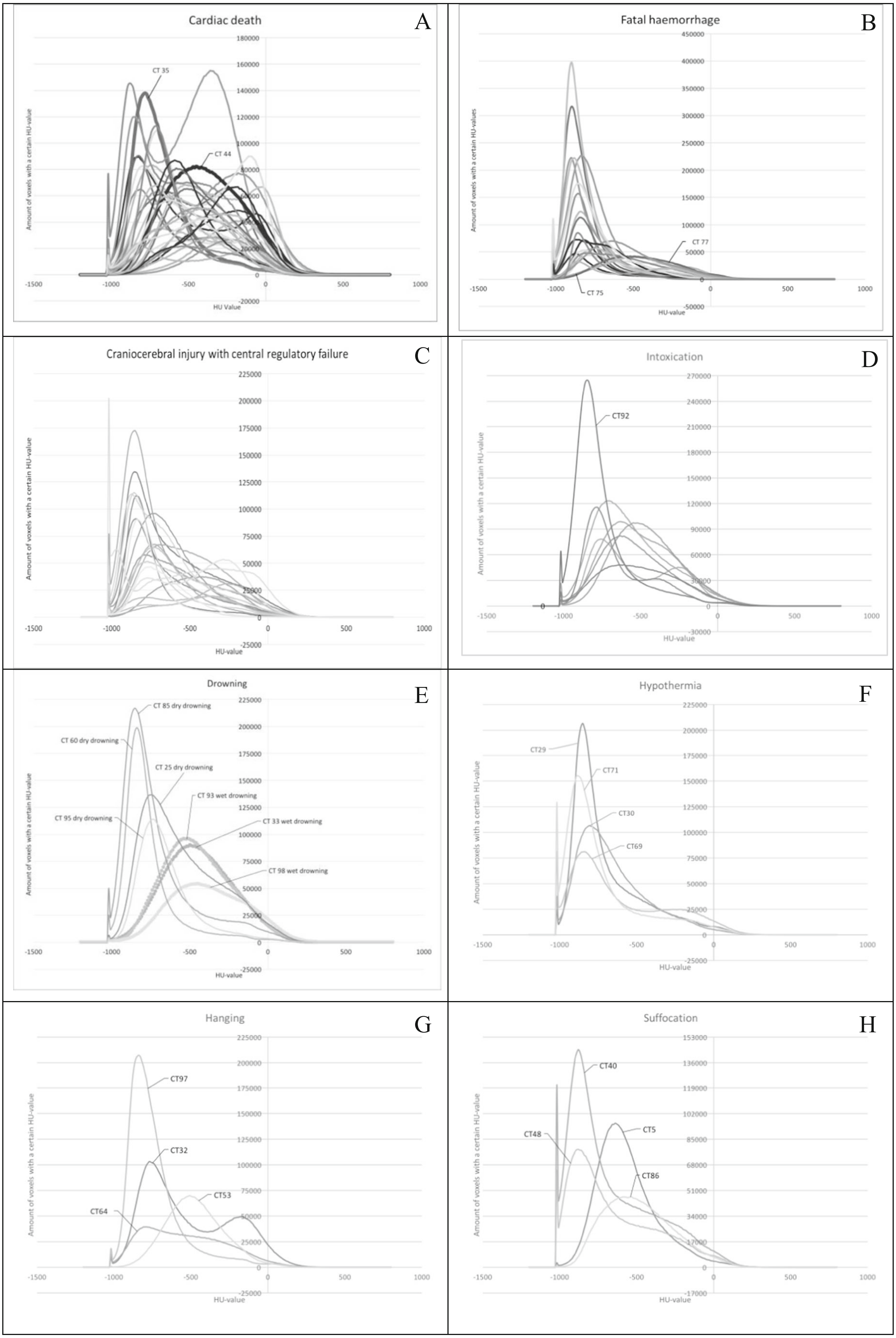
Cardiac death
A
CT 35
CT 44
Amount of voxels with a certain HU-value
HU Value
Fatal haemorrhage
B
CT 77
CT 75
Amount of voxels with a certain HU-values
HU-value
Craniocerebral injury with central regulatory failure
C
Amount of voxels with a certain HU-value
HU-value
Intoxication
D
CT92
Amount of voxels with a certain HU-value
HU-value
Drowning
E
CT 85 dry drowning
CT 60 dry drowning
CT 25 dry drowning
CT 93 wet drowning
CT 95 dry drowning
CT 33 wet drowning
CT 98 wet drowning
Amount of voxels with a certain HU-value
HU-value
Hypothermia
F
CT29
CT71
CT30
CT69
Amount of voxels with a certain HU-value
HU-value
Hanging
G
CT97
CT32
CT53
CT64
Amount of voxels with a certain HU-value
HU-value
Suffocation
H
CT40
CT48
CT5
CT86
Amount of voxels with a certain HU-value
HU-value

Suffocation

Suffocation as cause of death ($n = 4$) also showed rather varying curves (Fig. 2h). CT 40 and CT 48 appeared rather similar with a peak at −890 HU and a plateau with little decrease of values between −570 HU and −240 HU. CT 5 and CT 86 had a rather bell-shaped peak at −650 HU and −550 HU, respectively.

That caused the mean distribution curve to show two peaks (Fig. 3h). The first was at −850 HU and the second at −680 HU. After that, a steady decline was observed down to zero.

Discussion

The present study investigated the HU distribution curves of the lungs in PMCT exams using a semi-automatic segmentation tool for post-mortem CT data. It was hypothesized that the HU profiles of the lungs may be supportive in assessing the cause of death. The study population was divided into groups according to the cause of death as given within the autopsy reports. The study groups will be discussed separately.

Cardiac death

Cardiac death cases are regularly presenting with an acute pulmonary oedema and congestion. The increased amount of water and other blood components caused the mean radiopacity of the lung tissue to increase too. Therefore, the HU profiles in cardiac death cases presented with a broad occupation of all negative HU value ranges. Although water has per definition a HU value of 0, it is only rarely occupying an entire voxel in purity. That results in differently partial volume affected voxels distributed all over the entire negative HU range as the majority of voxels still have at least traces of air within the alveoli causing that no peak at 0 HU can be expected even when there is a lot of oedema within the lungs.

Shiotani et al. described a shift of HU values due to a post-mortem pulmonary oedema, which increases with time [19]. It is therefore possible that the observed shift in radiopacity may be influenced by post-mortem changes as well. Shiotani et al. only examined three cases, which all had a cardiac-related cause of death and received an unknown amount of volume administration prior to death. However, there may be an influence of the post-mortem interval on the specific appearance of the HU profiles, which has not been investigated within the present study.

Interindividual differences between the curves may be explained by the individual nature of the cardiac failure. For example, CT 44 (Fig. 2a) shows a case of cardiac failure after re-infarction during stenting, while CT 35 (Fig. 2a) shows a case of cardiac failure in a trauma case (traffic accident) with haemorrhage. From the autopsy perspective, the cause of death was given as cardiac failure in the context of the above mentioned, but the HU profile rather shows behaviour comparable to the fatal haemorrhage case group. Therefore, based on the study results, it can be retrospectively assumed that in this case the blood loss was probably the dominating factor leading to death and the cause of death would have been better assessed as fatal haemorrhage.

When comparing different cases, the total amount of voxels belonging to a specific HU range must be considered with care as different cases have different total lung volumes. Therefore, it is the shape of the profile that contains specific information and not the absolute height of any of the peaks.

Fatal haemorrhage

The reviewed cases of fatal haemorrhage ($n = 21$) presented with an obvious shift to lower radiopacity levels especially when compared to cardiac death cases. Besides two exceptions (case 75 and 77), the profile behaviour was very invariable. The loss of blood inversely caused the relative portion of air within the lungs to increase so that cases of fatal haemorrhage presented with a sharp peak at low HU values.

In case 75 and 77 (Fig. 2b), perimortal interventions have been performed, especially volume transfusions were administered. These interventions altered the HU profile appearance distinctively as the "water load" broadened the HU profile comparable to pulmonary oedema in cardiac failure cases.

Craniocerebral injury with central regulatory failure

This group showed a very inhomogeneous behaviour. Very different profiles were present within these 23 cases. Thereby, the fact that death by craniocerebral injury can be caused by various mechanisms is also represented in the variety of HU curve behaviours. Isolated head trauma e.g. gunshot to the head or a lethal head injury as part of a polytrauma do not affect the water content of the lungs the same way. Also relevant blood aspiration may occur or not, which would have an influence on the HU value behaviour. Furthermore, HU peaks at low values may indicate that also a relevant blood loss was present in a specific head trauma case. This was the case for several of the cases in this group as can be seen in Fig. 2c. As also for the fatal haemorrhage cases, the HU profiles within the lungs are very much depending on any peri-mortem volume administration. In this case, group cases

Fig. 3 Mean HU profiles for all causes of death. The *x-axis* corresponds to the value of HU; the *y-axis* corresponds to the amount of voxels with a certain HU value. **a** Cardiac death, **b** fatal haemorrhage, **c** craniocerebral injury with central regulatory failure, **d** intoxication, **e** drowning, **f** hypothermia, **g** hanging and **h** suffocation

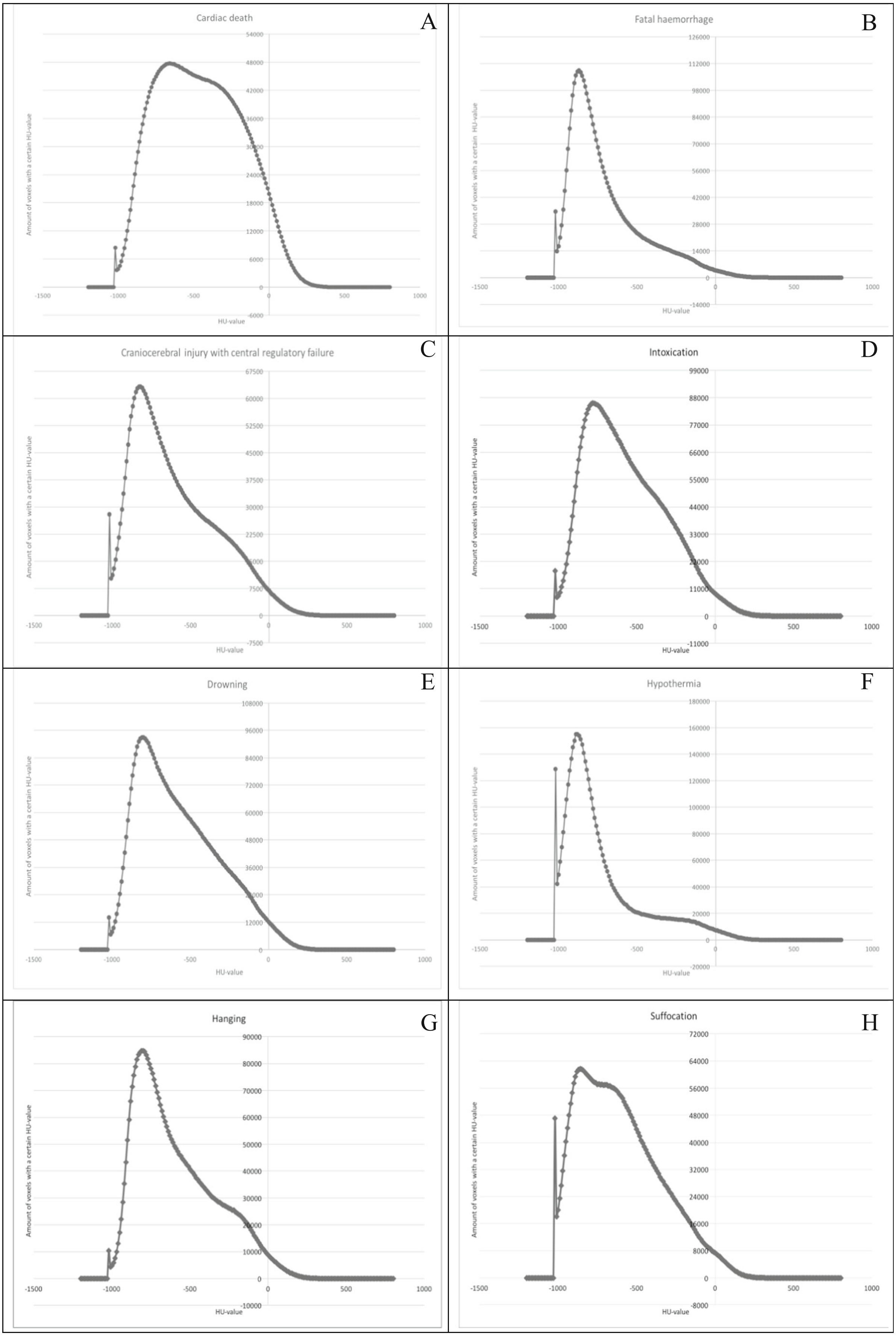
A
Cardiac death
54000
48000
42000
36000
30000
24000
18000
12000
6000
0
-6000
-1500
-1000
-500
0
500
1000
Amount of voxels with a certain HU-value
HU-value
B
Fatal haemorrhage
126000
112000
98000
84000
70000
56000
42000
28000
14000
0
-14000
-1500
-1000
-500
0
500
1000
Amount of voxels with a certain HU-value
HU-value
C
Craniocerebral injury with central regulatory failure
67500
60000
52500
45000
37500
30000
22500
7500
0
-7500
-1500
-1000
-500
0
500
1000
Amount of voxels with a certain HU-value
HU-value
D
Intoxication
99000
88000
77000
66000
55000
44000
33000
11000
0
-11000
-1500
-1000
-500
0
500
1000
Amount of voxels with a certain HU-value
HU-value
E
Drowning
108000
96000
84000
72000
60000
48000
36000
12000
0
-1500
-1000
-500
0
500
1000
Amount of voxels with a certain HU-value
HU-value
F
Hypothermia
180000
160000
140000
120000
100000
80000
60000
40000
20000
0
-20000
-1500
-1000
-500
0
500
1000
Amount of voxels with a certain HU-value
HU-value
G
Hanging
90000
80000
70000
60000
50000
40000
30000
20000
10000
0
-10000
-1500
-1000
-500
0
500
1000
Amount of voxels with a certain HU-value
HU-value
H
Suffocation
72000
64000
56000
48000
40000
32000
24000
16000
8000
0
-8000
-1500
-1000
-500
0
500
1000
Amount of voxels with a certain HU-value
HU-value

without any intervention as well as cases receiving intensive care were included.

Therefore, especially in the group of craniocerebral injury, the HU profiles are less related to the actual cause of death but rather to the specific pulmonary alteration occurring in the specific traumatic case circumstances.

Intoxication

In intoxication cases, pulmonary oedema was to be expected. Thereby, an HU profile distribution comparable to cardiac death cases can be explained. The mean distribution showed a shift of HU values to higher radiopacity levels especially when compared to hypothermia or the fatal haemorrhage cases.

CT 92 showed an exceptional behaviour with more than 250,000 voxels at around −850 HU, which was more than twice as much compared to a specific HU range of the other profiles. In this case, the graph showed a shift to lower values, which was a sign for the lag of the mentioned pulmonary oedema. In this particular case, the intoxication was caused by a respiratory paralysis due to methadone and morphine intoxication.

The mean distribution graph showed a shift to higher radiopacity values and would have been less peaky without the influence of CT 92.

Drowning

The drowning cases obviously presented with two different profile appearances (Fig. 2e). One peak dominated at low HU values and a second one rather bell shaped at higher values. Knowing from the autopsy room, there are two different types of drowning called dry or active and wet or passive drowning. Of course, there are mixed forms as well. However, dry drowning lungs are expected when the victim drowned actively being conscious, with all reflexes intact not aspirating but swallowing the drowning fluid. In contrast, wet drowning lungs are expected when the victim drowned rather passively by aspirating the drowning fluid without any laryngospasm and not swallowing.

These two different drowning types now experience a further support by the two different HU profile appearances of the drowning lungs. In active dry drowning, there are peaks at low HU values present, whereas passive wet drowning leads to broader rather bell-shaped profiles dominating higher HU values. The latter need an explanation for the absence of consciousness and reflexes, which may be provided by toxicological findings, trauma findings to the head or natural causes of death occurring while being in water. Comparing the autopsy findings, the four cases situated in lower HU areas represented dry drowning cases and the three localized in the higher HU regions were wet drowning cases.

As the diagnosis of drowning without aspiration has been questioned in the past and even been called a myth without foundation [20], a possible quantification of the amount of fluid in the lung using CT segmentation could provide a prove to clinicians that, indeed, there is a dry drowning.

Hypothermia

The hypothermia group was rather small with only four cases. However, the mean HU curve was dominated by a distinctive peak around −800 HU comparable to the fatal haemorrhage cases. This result is well in line with recent literature on post-mortem imaging of hypothermia cases [21, 22]. The aerated lung volume and the percentage of aerated lung volume are described as being greater in fatal hypothermia cases than in other causes of death. However, attention has to be paid to this finding when hypothermia was not the sole cause of death. Especially when a relevant blood loss promoted the drop of body core temperature, both circumstances may contribute to the special one peak appearance of the HU profile. Furthermore, it has to be taken into account the fact that hyperventilation contributes to the appearance of the HU profiles as well as to a certain amount to oedema in the death process too.

Hanging and suffocation

Both groups consisted of four cases only. In contrast to the hypothermia cases, the variability was very high in both groups. Therefore, serious conclusions should not be drawn from the results in these two case groups as larger study populations are needed first. So far, no specific appearance can be discussed on the basis of the four cases each. However, as these cases were investigated within the study, the results were presented as well.

Limitations

First of all, the sample size with 147 CTs is rather low, and almost 30 % of the cases had to be excluded e.g. due to artefacts within the images that were expected to affect the HU measurements. The authors feel that this may be a realistic percentage to be expected in forensic PMCT scans as they have a higher probability of artefact causing foreign bodies compared to e.g. clinical CT scans. Furthermore, the probability of severe thoracic trauma is also increased in forensic PMCT data. Therefore, one limitation may be that the method is only applicable in 70–80 % of the forensic cases.

While performing the study, it was also realized that the case groups as generated based on the cause of death assessment at autopsy may also cause problems. The cause of death assessment is often a final diagnosis considering a lot of morphologic findings and findings at the scene as well. The problem was complicated by the fact that in some cases also a combination of different potentially death causing findings were documented. Depending on the individual forensic pathologist, e.g. a case with severe head trauma (e.g. gunshot to the head) may be assessed as central regulatory failure and others rather discussed the severe blood loss as cause of death. Thereby, the case groups were not as homogeneous as expected regarding their autopsy morphology. This may be a limitation of the study. On the other hand, it also shows that the HU profiles of the lungs rather correlate to specific lung alterations and not as good to the cause of death as such. Thereby, the HU profiles can be used as additional hint for a specific lung alteration (congestion, oedema, blood loss) that may be interpreted differently considering other findings. As a good example, fatal haemorrhage and hypothermia may be mentioned. Both groups presented with comparable HU profiles, which are not really cause of death specific. However, knowing further autopsy findings and findings at the scene, the peaky profile can support either the diagnosis of fatal blood loss or fatal hypothermia and help separating from other possible causes of death.

Another limiting factor may be the fact that not for every case there was clear knowledge available about possible perimortal interventions. Resuscitation attempts or intravenous perfusions may have altered the water content of the lungs as well. This problem also applies to the medical history of the cases, which was not known for everyone. Therefore, clinical symptoms such as related to cardiac insufficiency, chronic obstructive pulmonary disease (COPD) or chemotherapy may affect the post-mortem CT behaviour of the lungs but cannot directly be assessed based on the post-mortem autopsy morphology only. Recent literature has also reported kV and body temperature dependencies of HU values, which may be negligible for the present study as the error should not exceed 10 HU [23].

Conclusions

HU profiles of the lungs segmented by Mia Lite can support specific causes of death by visualizing specific pulmonary alterations. Especially, cases of hypothermia and fatal haemorrhage differ from myocardial failure, and dry and wet drowning may be separated using the HU profiles of the lungs.

References

1. Roberts IS, Benamore RE, Benbow EW, Lee SH, Harris JN, Jackson A, Mallett S, Patankar T, Peebles C, Roobottom C, Traill ZC (2012) Post-mortem imaging as an alternative to autopsy in the diagnosis of adult deaths: a validation study. Lancet 379:136–142
2. Jackowski C (2013) Special issue on postmortem imaging 2013. Forensic Sci Int 225:1–2
3. Persson A, Lindblom M, Jackowski C (1987) (2011) A state-of-the-art pipeline for postmortem CT and MRI visualization: from data acquisition to interactive image interpretation at autopsy. Acta Radiol Stockh Swed 52:522–536
4. Scholing M, Saltzherr TP, Fung Kon Jin PHP, Ponsen KJ, Reitsma JB, Lameris JS, Goslings JC (2009) The value of postmortem computed tomography as an alternative for autopsy in trauma victims: a systematic review. Eur Radiol 19:2333–2341
5. Le Blanc-Louvry I, Thureau S, Duval C, Papin-Lefebvre F, Thiebot J, Dacher JN, Gricourt C, Touré E, Proust B (2013) Post-mortem computed tomography compared to forensic autopsy findings: a French experience. Eur Radiol 23:1829–1835
6. Michiue T, Sakurai T, Ishikawa T, Oritani S, Maeda H (2012) Quantitative analysis of pulmonary pathophysiology using postmortem computed tomography with regard to the cause of death. Forensic Sci Int 220:232–238
7. Arthurs OJ, Guy A, Kiho L, Sebire NJ (2015) Ventilated postmortem computed tomography in children: feasibility and initial experience. Int J Legal Med 129:1113–1120
8. Schulze C, Hoppe H, Schweitzer W, Schwendener N, Grabherr S, Jackowski C (2013) Rib fractures at postmortem computed tomography (PMCT) validated against the autopsy. Forensic Sci Int 233:90–98
9. Jackowski C, Thali M, Sonnenschein M, Aghayev E, Yen K, Dirnhofer R, Vock P (2004) Visualization and quantification of air embolism structure by processing postmortem MSCT data. J Forensic Sci 49:1339–1342
10. Egger C, Vaucher P, Doenz F, Palmiere C, Mangin P, Grabherr S (2012) Development and validation of a postmortem radiological alteration index: the RA-Index. Int J Legal Med 126:559–566
11. Dedouit F, Telmon N, Costagliola R, Otal P, Florence LL, Joffre F, Rougé D (2007) New identification possibilities with postmortem multislice computed tomography. Int J Legal Med 121:507–510
12. Sidler M, Jackowski C, Dirnhofer R, Vock P, Thali M (2007) Use of multislice computed tomography in disaster victim identification—advantages and limitations. Forensic Sci Int 169:118–128
13. Ward HE, Clarke BE, Zimmerman PV, Cleary MI (2002) The decline in hospital autopsy rates in 2001. Med J Aust 176:91
14. Jackowski C, Grabherr S, Schwendener N (2013) Pulmonary thrombembolism as cause of death on unenhanced postmortem 3T MRI. Eur Radiol 23:1266–1270
15. Jackowski C, Schwendener N, Grabherr S, Persson A (2013) Postmortem cardiac 3-T magnetic resonance imaging: visualization of sudden cardiac death? J Am Coll Cardiol 62:617–629
16. Geller SA (1984) Religious attitudes and the autopsy. Arch Pathol Lab Med 108:494–496
17. http://www.osirix-viewer.com/. 2015.
18. http://www.mia-solution.com/. 2015.
19. Shiotani S, Kobayashi T, Hayakawa H, Kikuchi K, Kohno M (2011) Postmortem pulmonary edema: a comparison between immediate and delayed postmortem computed tomography. Leg Med Tokyo Jpn 13:151–155
20. Orlowski JP, Szpilman D (2001) Drowning. Rescue, resuscitation, and reanimation. Pediatr Clin North Am 48:627–646
21. Schweitzer W, Thali M, Giugni G, Winklhofer S (2014) Postmortem pulmonary CT in hypothermia. Forensic Sci Med Pathol 10:557–569
22. Hyodoh H, Watanabe S, Katada R, Hyodoh K, Matsumoto H (2013) Postmortem computed tomography lung findings in fatal of hypothermia. Forensic Sci Int 231:190–194
23. Zech W-D, Jackowski C, Buetikofer Y, Kara L (2014) Characterization and differentiation of body fluids, putrefaction fluid, and blood using Hounsfield unit in postmortem CT. Int J Legal Med 128:795–802